Predicting Steady Lift and Drag Coefficient of Tandem aircraft using Prandtl's Extended Lifting-Line Theory implemented under ASWING

R. JAN (ISAE-SUPAERO)*, J-P.Condomines (ENAC),J-M. Moschetta(ISAE-SUPAERO)

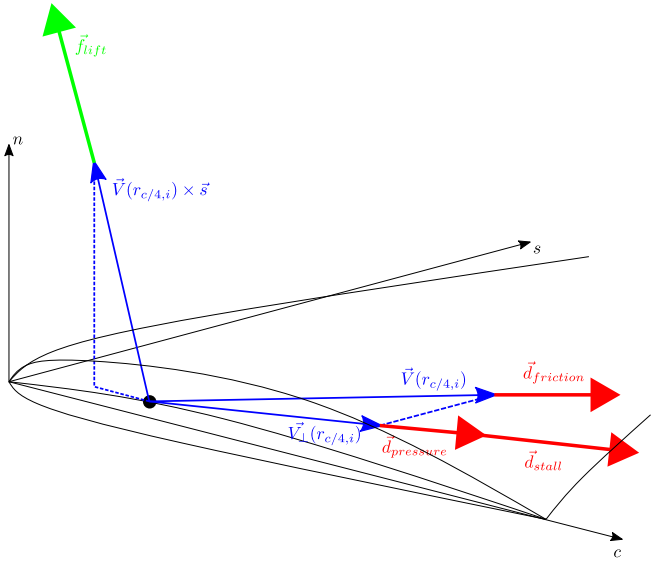

Figure 1: Wing : Lift and drag contributions in the local csn frame

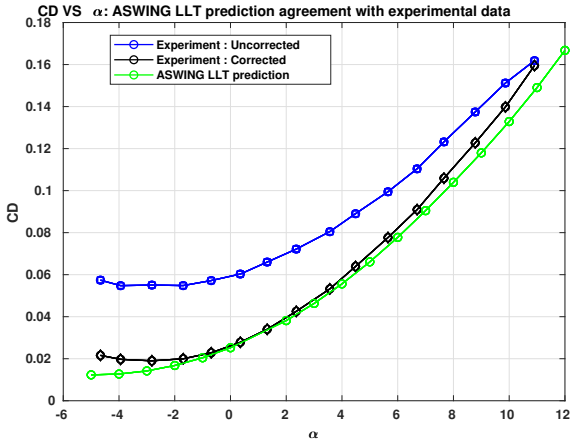

Figure 2: Aircraft 1 : CD VS α agreement between Aswing's LLT and corrected experimental data

1 Introduction

2 Extended Non linear lifting line theory for multiple lifting surface configuration

2.1 Aerodynamic loads:

In ASWING the lift generated by a surface beam is given by the unsteady form of Kutta Jukowski theorem, however here, one will only recall the steady part of it in equation 1. $\vec{V}$ denotes the local net stream velocity evaluated at horseshoes boundary position .

$$\vec{f}_{\text{lift}} = \rho \Gamma \vec{V} \times \hat{s} \tag{1}$$

where Γ is the circulation given by :

$$\Gamma(s) = \sum_{k=1}^{K} A_k \sin\left(k \arccos\left(\frac{s}{s_{\max}}\right)\right) \tag{2}$$

For the next sections, $\vec{V}$ must be concidered as the local stream veocities and its expression is given by

$$\vec{V}(\vec{r}) = \vec{V}_{\infty} - \vec{\Omega} \times \vec{r} + \vec{V}_{\text{ind}}(\vec{r}) + \vec{V}_{\text{gust}}(\vec{r}) - \vec{v}(\vec{r}) \tag{3}$$

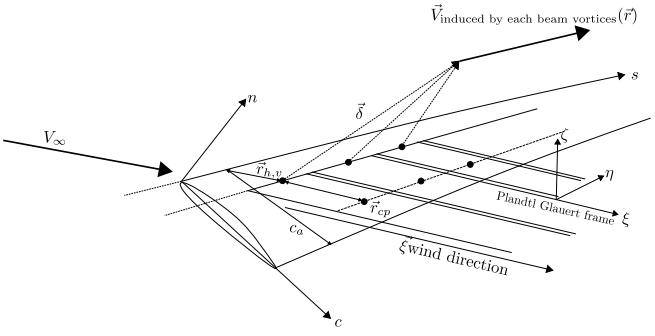

Figure 3: Induced velocity from bound vortices and circulation mode represented by wind aligned trailing vorticities

*Email address(es): romain.jan@isae-supaero.fr

where $\vec{V}_{\text{ind}}$ embeds the velocity influence of vortices, beam volume and engine jets. In the case of that paper some terms in 3 vanish like the first one because one will presented results for an anchored aircraft (restricted static movement). Moreover the last term vanishes aswell because it account for the unsteady effect of the local beam nodes deflection. Finally no gust will be concidered in that study so 3 becomes:

$$\vec{V}(\vec{r}) = \vec{V}_{\infty} + \vec{V}_{\text{ind}}\,(\vec{r}) \tag{4}$$

with defines as $\vec{V}_{\text{ind}}$

$$\vec{V}_{\text{ind}}(\vec{r}) = \sum_{k=1}^{K} \vec{v}_k(\vec{r}) A_k + \vec{w}_{\text{vol}}(\vec{r}) V_{\infty} \tag{5}$$

In the next section $\vec{V}$ will be evaluated at different positions but remains defined by the same expression.

Note that the cross product $\vec{V} \times \hat{s}$ imposes the lift to lay in the local cn plane as shown in figure 1
The lift generated by a fuselage beam is given by the steady form of the slender body theory:

$$\begin{aligned} \vec{f}_{\text{lift}} &= \rho \vec{V}_{\perp} (\vec{V} \cdot \hat{s}) 2\pi R \frac{dR}{ds} \\ \vec{V}_{\perp} &= \vec{V} - (\vec{V} \cdot \hat{s}) \hat{s} \end{aligned} \tag{6}$$

$\vec{V}_{\perp}$ the local stream veocity component in the cn plane. $\vec{V}_{\perp}$imposes the direction of the lift force as described in figure 5. In the case of a fuselage beams, the velocities vector is evaluated at the center of the cross section at position $r\vec{O}_i$ where i denotes the beam nodes index. Note that if the cross section does not vary over the beam arc, the fuselage beam wont generate any lift.

Regarding the drag forces, one must denotes aswell surface and fuselage beams. The surface beam drag is expressed by equation 7 and is composed of 3 terms. A friction drag component, a pressure drag and a post stall contributions. The direction of thoses forces are imposed by the local nornal and net velocities evaluated at horseshoe vortex boundaries positions $\vec{r}_{h,v}$ as depicted on figure 1. cd_f and cdp can be obtain thanks to XFOIL software by interpolating the data in the linear range of angle of attack. The post stall contribution will be treated in the later related section.

$$\begin{aligned} \vec{f}_{\text{drag}} &= \frac{1}{2}\rho |\vec{V}| \vec{V} \bar{c} c_{d_f} + \frac{1}{2}\rho \left|\vec{V}_{\perp}\right| \vec{V}_{\perp} \bar{c} c_{d_p} \\ &\quad + 2\rho \frac{\vec{V}_{\perp}}{\left|\vec{V}_{\perp}\right|} (\vec{V} \cdot \hat{n})^2_{c.p.} \bar{c} \\ \vec{f}_{\text{drag}} &= \vec{d}_{friction} + \vec{d}_{pressure} + \vec{d}_{poststall} \end{aligned} \tag{7}$$

For fuselage beams, there are only a friction and pressure contribution denoted by the equation 8 *cdf* and *cdp* are the skin friction and the drag coefficient of a cylinder.

$$\begin{aligned} \vec{f}_{\text{drag}} &= \frac{1}{2}\rho |\vec{V}| \vec{V} 2R c_{d_f} + \frac{1}{2}\rho \left|\vec{V}_{\perp}\right| \vec{V}_{\perp} 2R c_{d_p} \\ &= \vec{d}_{friction} + \vec{d}_{pressure} \end{aligned} \tag{8}$$

The pressure and skin friction are described on figrue 5 c_{d_f} and c_{d_p} are the skin friction and the drag coefficient of a cylinder. c_{d_p} varies from 1.4 to 0.2 depending of the Reynold number but for UAV applications, one would prefer 1.2. Regarding the skin friction drag one can use the 2 empircal Blasius formulas recalled by 9. Depending on where the propeller is place on the geometry, one would advice the turbulent formula for propeller placed near or on fuselage beam.

$$\begin{aligned} C_{f-\text{ laminar}} &= \frac{1.328}{\sqrt{Re_l}} \\ C_{f-\text{ turbulent}} &= \frac{0.427}{[\log Re_l - 0.407]^{2.64}} \end{aligned} \tag{9}$$

Regarding aerodynamic forces, one won't go futher because the paper does not aim at providing a stability analysis. The reader must have in mind, that ASWING's model computes the local aerodynamic momentum contributions of the lift, drag and 2D cm profile.

2.2 Prandtl-Glauert Transformation for compressibility effect:

In order to compute aerodynamic loads, one must solve the discrete lifting line theory. However one solves it in the Prandtl-Glauert space to account for compressibility effect. Consequently the trailing edge of the horseshoes are windaligned as described on figure 3. The Prandtl-Glauert axis given by equation 10

$$\begin{Bmatrix} \xi \\ \eta \\ \zeta \end{Bmatrix} = \begin{bmatrix} \bar{P} \end{bmatrix} = \begin{Bmatrix} x \\ y \\ z \end{Bmatrix} \tag{10}$$

$$\begin{aligned} \bar{P} &= \begin{bmatrix} \dots & \vec{\xi}^T & \dots \\ \dots & \hat{\eta}^T & \dots \\ \dots & \hat{\zeta}^T & \dots \end{bmatrix} \\ &= \begin{bmatrix} \frac{1}{\lambda}\cos\alpha\cos\beta & -\frac{1}{\lambda}\sin\beta & \frac{1}{\lambda}\sin\alpha\cos\beta \\ \cos\alpha\sin\beta & \cos\beta & \sin\alpha\sin\beta \\ -\sin\alpha & 0 & \cos\alpha \end{bmatrix}_{\text{wind}} \end{aligned} \tag{11}$$

where $= \sqrt{1 - M^2_{\text{PG}}}$ is the stretching scalar. The Prandtl-Glauert Mach number is actually the real infinite Mach number. Finally $\vec{\xi}$ is aligned with the wind

direction as illustrated by figure 3 and equation 12

$$\vec{\xi} = \frac{1}{\sqrt{1-M_{\mathrm{PG}}^2}} \left\{ \begin{array}{c} \cos\alpha\cos\beta \\ -\sin\beta \\ \sin\alpha\cos\beta \end{array} \right\}_{\mathrm{wind}} \tag{12}$$

Proceding to this transformation reovers a compressible flow problem in the transform state space which can be integrated to get the influence velocities function of vortices and volumes.The equation 13 states the transform prblem.

$$\begin{array}{c} (1-M_{\mathrm{PG}}^2)\dfrac{\partial^2\phi}{\partial x^2}+\dfrac{\partial^2\phi}{\partial y^2}+\dfrac{\partial^2\phi}{\partial z^2}=0 \\ \downarrow \\ \dfrac{\partial^2\phi}{\partial \xi^2}+\dfrac{\partial^2\phi}{\partial \eta^2}+\dfrac{\partial^2\phi}{\partial \zeta^2}=0 \end{array} \tag{13}$$

The velocities in the cartesian space is then obtain ("stretched back") with transposal P matrix as it is a rotation one.

$$\begin{aligned} \left\{ \begin{array}{c} \partial\phi/\partial x \\ \partial\phi/\partial y \\ \partial\phi/\partial z \end{array} \right\} &= \left[\begin{array}{ccc} \xi_x & \eta_x & \zeta_x \\ \xi_y & \eta_y & \zeta_y \\ \xi_z & \eta_z & \zeta_z \end{array} \right] \left\{ \begin{array}{c} \partial\phi/\partial\xi \\ \partial\phi/\partial\eta \\ \partial\phi/\partial\zeta \end{array} \right\} \\ &= \left[\begin{array}{c} \bar{P}^T \end{array} \right] \left\{ \begin{array}{c} \partial\phi/\partial\xi \\ \partial\phi/\partial\eta \\ \partial\phi/\partial\zeta \end{array} \right\} \end{aligned} \tag{14}$$

Note that the streching factor λ tends to zero with Mach number reachs 1. This transformation thus diverges in the surrounding of transonic flow. It will however recover correctlty the compressibility effect of flow up to $M_\infty = 0.7$

2.3 Vortex influence function:

Circulations modes are solved by integrate the Biot Savart law over the circulation of all beams. The discrete bound are placed at quater chord in each local cn plane and the trainling legs are aligned with the wind direction. The modal contribution of each circulation mode is given by 15

$$\begin{array}{l} \Gamma_k = A_k \sin\left(k \arccos\left(\dfrac{s_a}{s_{max}}\right)\right) \\ \text{where} \quad \theta_a = \dfrac{1}{2}\left(\theta_i + \theta_{i+1}\right) \end{array} \tag{15}$$

where θ_a is an averaged mid point and the averaged interpolated position is given by:

$$\vec{r}_a = \vec{r}_i + \left(\vec{r}_{i+1} - \vec{r}_i\right)\frac{s_a - s_i}{\Delta s} \tag{16}$$

As mentionned earlier, the position of the horseshoe bound vortices is downstream from a quarter chord in the wind direction as shown on figure 3

$$\vec{r}_{h.v.} = \vec{r}_a + \frac{\bar{c}/4 - \bar{x}_o}{|\vec{\xi}\times\hat{s}|}\vec{\xi} \tag{17}$$

And the control points are aswell downstream from approximatetly half a chord distance in the wind direction

$$\vec{r}_{c.p.} = \vec{r}_{h\cdot v.} + \frac{h\bar{c}_a}{|\vec{\xi}\times\hat{s}|}\vec{\xi} \tag{18}$$

where h is defined by:

$$h = \frac{1}{4\pi}\frac{dc_\ell}{d\alpha} \tag{19}$$

with $\frac{dc_\ell}{d\alpha}$ is the 2D local slope of the airfoil.

The velocity induced by vortices are then obtained by integrating the Biot-Savart law in the Prandtl-Glauert space to account for compressibility effect and bring back to the physical space using the transformation matrix:

$$\begin{aligned} \vec{v}_k(\vec{r}) &= \left[\begin{array}{c} \bar{P} \end{array} \right] \left\{ \begin{array}{c} \partial\phi/\partial\xi \\ \partial\phi/\partial\eta \\ \partial\phi/\partial\zeta \end{array} \right\}_k (\vec{r}) \\ &= \left[\begin{array}{c} \bar{P}^T \end{array} \right] \left\{ \frac{1}{4\pi}\sum_{i=1}^{I-1} \sin\left(k\theta_a\right) \int \frac{d\vec{\ell}\times\vec{\delta}}{\delta^3} \right\} \end{aligned} \tag{20}$$

with:

$$d\vec{\ell} = d\vec{r}_P = \overline{\overline{P}}\, d\vec{r}$$

where $\vec{\delta}(\vec{r})$ is the relative vector between the position where the induced veolicty must be evaluated and the position of a small element on the bound or trainling horseshoe.

$$\vec{\delta} = \vec{r}_P - \vec{r}_P(\ell) = \overline{\overline{P}}\left\{\vec{r} - \vec{r}_{(\ell)}\right\}$$

$$\vec{v}_k = \left[\bar{P}^T\right] \left\{ \frac{1}{4\pi}\sum_{i=1}^{I-1} \sin\left(k\theta_a\right) \int \frac{d\vec{\ell}\times\vec{\delta}}{\left(\delta^2+\varepsilon^2\right)^{3/2}} \right\} \tag{21}$$

Note that aligning the trailing vorticies with the freestream direction gives better accuracy for high angle of attack and sideslip, because the votices are sheded by the wind and are no more with the local csn frame.

2.4 Volume influence function:

Using source/length and doublet/length defined by equations 22, one can recover the volume contribution to induced velocity. Indeed they impose the flow tangency on the circular beam of cross sectionnal radius R.

Densities are given in the Prandtl-Glauert frame to take into account compressibility effects.

$$\sigma(\ell) = \frac{d\left(\pi R^2\right)}{d\ell}(\vec{\xi}\cdot\hat{\ell})\vec{\nu}(\ell) = 2\pi R^2(\vec{\xi} - (\vec{\xi}\cdot\hat{\ell})\hat{\ell}) \quad (22)$$

The induced velocity is then given by the integrated Biot Savart law for both densities and given by equation 23

$$\begin{aligned}\vec{w}_{\text{vol}}(\vec{r}) = \left[\ \bar{P}^T\right]\Bigg\{\frac{1}{4\pi}\int\Bigg[&\frac{\sigma\vec{\delta}}{\left(\delta^2+\varepsilon^2\right)^{3/2}}\\ &+\frac{\vec{\nu}\delta^2 - 3(\vec{\nu}\cdot\vec{\delta})\vec{\delta}}{\left(\delta^2+\varepsilon^2\right)^{5/2}}d\ell\end{aligned} \quad (23)$$

where δ is the relative vector between $\vec{r}$ (where $\vec{w}_{\text{vol}}$is evaluated) and $\vec{r}(l)$ the position of each densities. δ is expressed in the Prandtl-Glauet frame, because the overall integration is done in that space as mentionned earlier. Equations 23 and 22 can be used to recover the thickness effect of a wing, by setting the local Radius as half of the maximum airfoil thickness. Volumic effects are mostly evaluated for fuselage which are usually wider than wings.

2.5 Separation and Stall modeling:

Stall and separation are modeled based on finite swept wing theory. It results in a non zero normal velocity in the Kutta flow tangency condition described by

$$\vec{V}\left(\vec{r}_{c.p.}\right)\cdot\hat{n}_{c.p.} - \frac{V_\perp}{4\pi h}K_{\text{s}}f_{\text{stall}}\left(c_\ell\right) = 0 \quad (24)$$

where f_{stall} is a post stall function :

$$f_{\text{stall}} = \Delta c_\ell \log\frac{1+\exp\left[\left(c_\ell - c_{\ell_{\max}}\right)/\Delta c_\ell\right]}{1+\exp\left[\left(c_{\ell_{\min}} - c_\ell\right)/\Delta c_\ell\right]} \quad (25)$$

This function aims at modifying the 2D lift slope as followed

$$\frac{dc_\ell}{d\alpha} \simeq \begin{cases} 4\pi h, c_{\ell\,\min} < c_\ell < c_{\ell_{\max}} \\ 4\pi h/\left(1+K_{\text{s}}\right), c_\ell < c_{\ell\,\min}, c_{\ell\,\max} < c_\ell \end{cases} \quad (26)$$

At the light of the separation, the non respected flow tangency condition implies a pressure profile additionnal drag

$$\begin{aligned} c_d &= 4\left(\frac{\vec{V}\cdot\hat{n}}{V}\right)^2 \\ &\simeq 4\left(\frac{K_{\text{s}}}{1+K_{\text{s}}}\right)^2\left(\sin\alpha - \frac{c_{\ell\,\max}}{4\pi h}\right)^2, c_\ell > c_{\ell_{\max}} \end{aligned} \quad (27)$$

The reader must aknowledge that cl won't fall back after but reach an asymptot, which is not obviously accurate with physic behaviour. However it is very interesting for near and early stall. The user do not recommand the study for extreme angle of attack.

2.6 Ciculation coefficient constraints

Denoting K the number of ciculation modes of all the lifting surfaces, one must provides K constraints equations to solves the overall problem. Those are imposed by the modified Kutta condiion of flow tangency on the surface at each discrete control points given by equation 28

$$\vec{V}\left(\vec{r}_{c.p.}\right)\cdot\hat{n}_{c.p.} - \frac{V_\perp}{4\pi h}K_{\text{s}}f_{\text{stall}}\left(c_\ell\right) = 0 \quad (28)$$

The quasi normal vector $\hat{n}_{c.p.}$ is defined by

$$\hat{n}_{cp.} = \bar{T}^T\begin{Bmatrix}\sin\alpha_A \\ 0 \\ \cos\alpha_A\end{Bmatrix} \quad (29)$$

where α_A embed the effect of flaps local twist and zero lift angle of attack:

$$\alpha_A = \alpha_{Ao} + \frac{dc_\ell/d\delta_{p_1}}{dc_\ell/d\alpha}\delta_{p_1} + \frac{dc_\ell/d\delta_{p_2}}{dc_\ell/d\alpha}\delta_{Y_2}\ldots \quad (30)$$

Note that the second term account reasonably for separation and stall. A more detailed expression of 28 gives :

$$\begin{aligned}&\sum_{i=1}^{I-1}\left(\vec{V}\left(\vec{r}_{c.p.}\right)\cdot\hat{n}_{c.p.}\right)_a\sin\left(k\theta_a\right)\Delta\theta \\ &-\frac{V_\perp}{4\pi h}K_{\text{s}}f_{\text{stall}}\left(c_\ell\right) = 0 \quad k\in[1\ldots K]\end{aligned} \quad (31)$$

Recalling $\vec{V}\left(\vec{r}_{c.p.}\right)$ expresion (3) and (5), it includes the vortex influence functions that contains the ciculation modes. Consequently one gets K well constraints equations allowing the solution of the overall problem.

3 Experimental and CFD comparison with ASWING's LLT

Lift and Drag coefficient prediction of ASWING' steady LLT must be compared with experimental and CFD data. Moreover one must seek the most interactive case to ensure that the presented theory results predicts correctly even in the worst case. Consequently, the tandem confifuration is very accurate because, there is a lot of interaction and impact between each wings and their respected generated vortices. [Nasa Technical report] provides a set of data for 4 differents tandem wing configuration. The tandem congfiguration is described by figure [Insérer schéma tandem]. The experimental campagn has been run in a 2 by 3 meters low Reynold, closed throat wind tunnel. The tab [Insérer tab] sum up

	Tandem aircraft 1	Tandem aircraft 2
Airfoil	NASA-GAW2	NACA4309
Speed	V = 69.15m/s	V = 30m/s
Re	1.4E6	2.65E5
Planform	Rectangular	Rectangular
c_{canard}	0.22m	0.129m
c_{wing}	0.305m	0.129m
b_{wing}	1.83m	2.0425m
b_{canard}	1.29m	2.1805m
ϑ_{canard}	2	0
ϑ_{wing}	0	0
G (gap)	$+0.5c_{wing}$	-0.101m
S (Stagger)	$1.63c_wing$	0.89m
S_{ref}	0.56m	0.544767m^2
Airframe	No	Yes

Table 1: Aircrafts' characteristic for ASWING's LLT validation

	NASA-GAW2		NACA4309
Re	9E5	1.4E6	2.65E5
cl_{alpha}	6.20	6.20	6.11
CL_{max}	1.5	1.7	1.2
CL_{min}	-0.5	-0.7	-0.3
$\alpha_{L=0}$	-4.25	-4.25	-3.9
cd_f	0.006	0.006	0.006
cd_p	0.002	0.002	0.0140

Table 2: Airfoil 2D approximated data

the main physical property of the experiment. Unfortunatly, the report only proides 1 set of corrected data. However, it is the worst case as it is the one for positive gap and minimum stagger.

4 Parametric Study of Tandem aircraft with high aspect ratio quasi eliptical planform

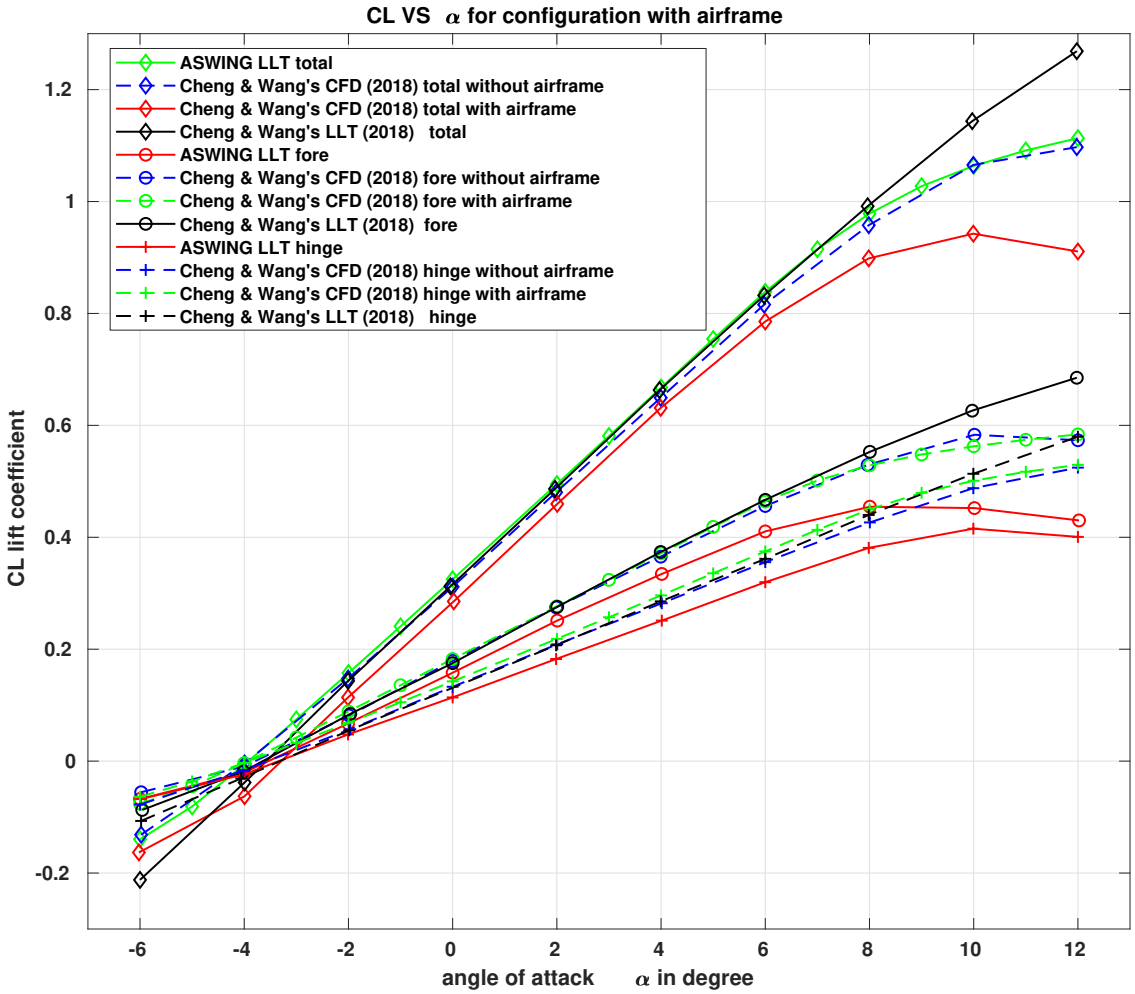

Figure 4: Aircraft 2 : CL VS α, agreement between ASWING'LLT and CFD result for 2 cases : with and without the airframe on Cheng and Wang's Tandem aircraft

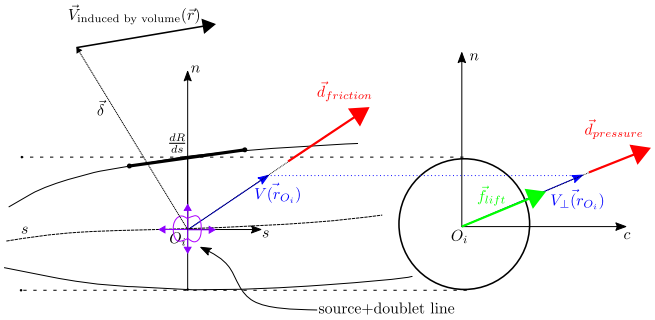

Figure 5: Fuselage : Lift, drag contributions and volume influence on local velocity

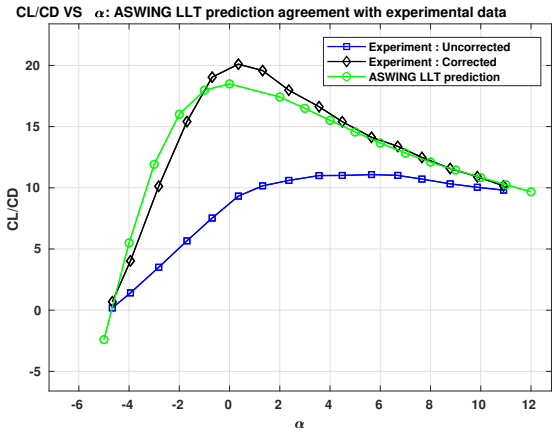

Figure 6: Aircraft 1 : CL/CD VS α agreement between Aswing's LLT and corrected experimental data

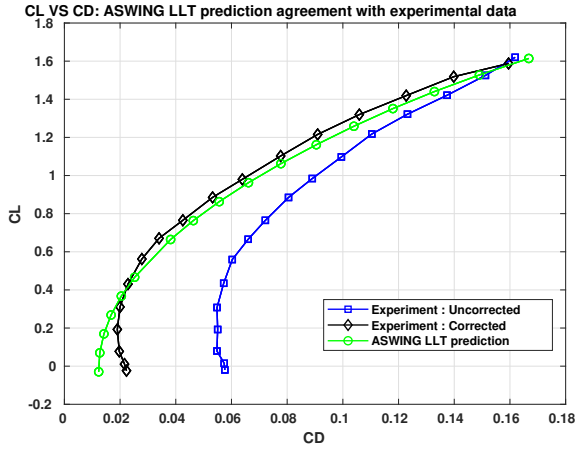

Figure 7: Aircraft 1 : CL VS CD agreement between Aswing's LLT and corrected experimental data

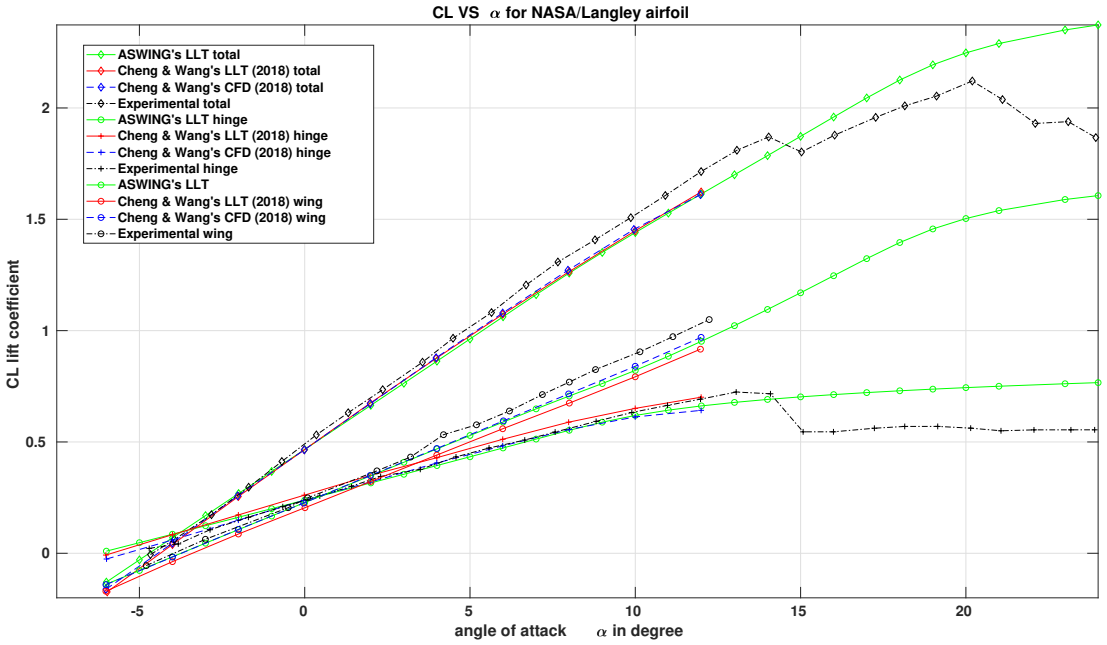

Figure 8: Caption

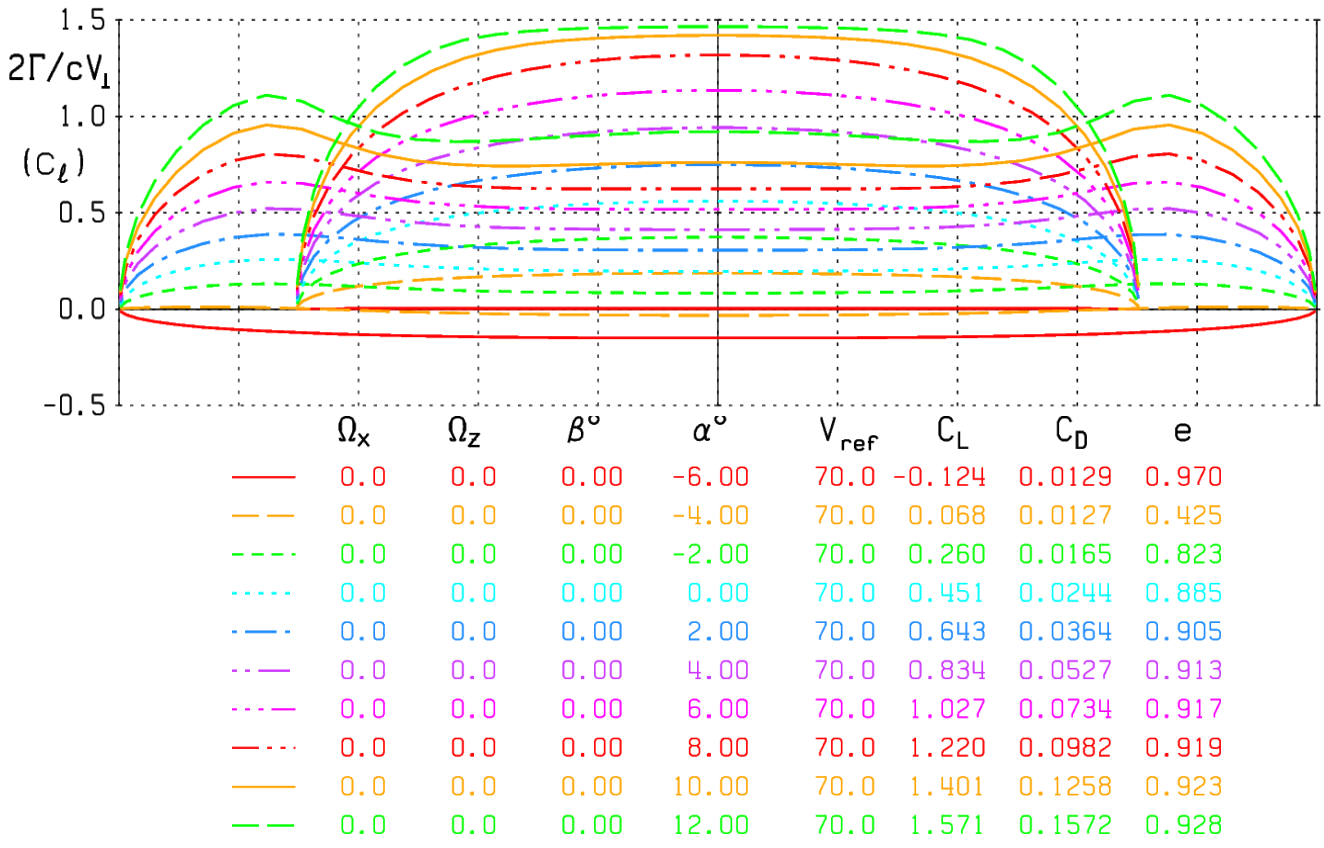

Figure 9: Effect of angle of attack on each local 2D corrected lift coefficient Cl(y) for aircraft 1